Available online at www.sciencedirect.com
SCIENCE DIRECT®
ELSEVIER
International Journal of Solids and Structures 43 (2006) 1832–1853
INTERNATIONAL JOURNAL OF SOLIDS and STRUCTURES
www.elsevier.com/locate/ijsolstr

Design of patterned multilayer films with eigenstrains by topology optimization

Joseph M. Pajot [a], Kurt Maute [a,*], Yanhang Zhang [b], Martin L. Dunn [b]

[a] *Department of Aerospace Engineering and Sciences, University of Colorado at Boulder, Boulder, CO 80309-0429, USA*
[b] *Department of Mechanical Engineering, University of Colorado at Boulder, Boulder, CO 80309-0429, USA*

Received 6 December 2004; received in revised form 10 March 2005
Available online 19 April 2005

Abstract

We develop a formal approach to design shaped microstructures from multilayer films with eigenstrains in the layers. The eigenstrains are inelastic strains that vary from layer to layer resulting in elastic misfit between the layers. Examples include thermal expansion mismatch between the layers, piezoelectric strains, and strains in shape memory alloys. In our approach, the eigenstrains are manipulated by spatially patterning the films to generate structures that, although fabricated by a conventional, planar thin film technology, deform into desired three-dimensional shaped surfaces. The material patterns in the individual layers are determined by topology optimization allowing the creation of arbitrarily complex, geometric layouts. In contrast to existing topology optimization methods for patterning plate structures, the goal of the proposed approach is to generate large deformations via eigenstrains, rather than to increase the stiffness of plate via reinforcement patterns. The optimization methodology is demonstrated by the design of two- and three-layer thin film structures. The performance of the optimized designs is verified by experiments showing the importance of accounting for a nonlinear kinematics in order to obtain the desired shape in the deformed configuration. While our approach is demonstrated in the context of the design of three-dimensional microstructures, it can be easily applied to a variety of problems where it is desired to control the complex shape of plate-like structures by spatial actuation—the spatial actuators are represented by eigenstrains.

Keywords: Multilayer film; Shaped surfaces; Topology optimization

* Corresponding author. Tel.: +1 303 735 2103; fax: +1 303 492 4990.
E-mail address: maute@pegasus.colorado.edu (K. Maute).

0020-7683/$ - see front matter © 2005 Elsevier Ltd. All rights reserved.
doi:10.1016/j.ijsolstr.2005.03.036

1. Introduction

Over the past 15 or so years the advancement of microsystems technology has largely been fueled by processing innovations. For example, the increased number of structural layers available in polysilicon surface micromachining, due to the introduction of chemical mechanical polishing processes, has led to additional degrees of freedom for the designer, resulting in microsystems with increased functionality and complexity. A large class of microsystems fabrication technologies, for example bulk and surface micromachining, are now quite mature as evidenced by the number of commercial foundry services available. The stability of this fabrication infrastructure is such that it makes sense for structural innovations to proceed and systematic approaches that manipulate established technologies to be pursued.

With a few notable exceptions, microsystems technologies are primarily based on the addition or removal of material in two-dimensional patterned layers. As a result, three-dimensional structures are rare, and quite challenging to fabricate. They offer the promise, though, of providing substantial extra freedom for designers, thus opening the door to numerous potential applications. One approach to three-dimensional microstructures involves complete three-dimensional fabrication technologies (Xia and Whitesides, 1998; Brittain et al., 2001), but is still very much in the research stage. An alternative approach which leverages the maturity of planar fabrication technologies is to maneuver two-dimensional structures into three-dimensional positions using the surface tension forces of polymers and/or metals in a liquid state prior to solidification (Harsh et al., 1999; Syms et al., 2003).

Even more design flexibility can be obtained if one can assemble curved, or shaped, plates into three-dimensional structures instead of just flat ones. Attaining a shaped surface is prohibitively difficult with existing MEMS design and fabrication paradigms that are based on planar thin film technologies. However, one possible approach arises from the realization that although many fabrication technologies are planar, they incorporate multiple layers of different materials that can be deposited in a spatially prescribed manner. Eigenstrains within the layers, which may vary spatially in the plane, will cause deformation of the planar structure. This deformation, most notably curvature of the structure, is often considered detrimental, but if used in a clever manner it can be beneficial.

An interesting example where eigenstrains are both beneficial and detrimental is shown in Fig. 1 where a gimbaled micromirror structure is suspended above a silicon substrate. The 500 μm diameter micromirror consists of a polycrystalline silicon film covered by a thin gold film to achieve the necessary optical reflectivity. To meet optical system requirements, the deviation from perfect flatness of the micromirror must be less than about 10% of the wavelength of light. Here, deformation of the multilayer mirror due to the eigenstrains is undesirable. This mirror is electrostatically controlled and must be assembled to sit above a silicon

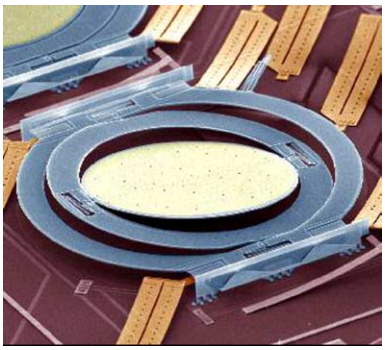

Fig. 1. SEM photograph of a 500 μm circular micromirror. The bimorph beams seen self-assemble the mirror to liftoff above the substrate (www.bell-labs.com).

substrate after fabrication. This placement is accomplished by bimaterial beam actuators, which also consist of a gold film on polysilicon. These actuators deform due to the eigenstrains, here due to thermal expansion mismatch between the gold and polysilicon and intrinsic growth stresses. In Fig. 1, the gimbaled micromirror structure is pictured suspended above the substrate by the attached bimaterial beams. In the case of the support beams, the deformation from the eigenstrains is desirable.

While microsystems technologies provide a wealth of applications for thin-film microstructures with prescribed shapes, there are many other technological arenas at macroscopic scales that can profit from the ability to locally control the shape of plate-like structures via eigenstrains. Examples include plate and shell structures with patches of active materials such as shape memory alloys or piezoelectric ceramics (Wang et al., 1997; Lin and Ren, 1998; Wang and Wang, 2000; Quek et al., 2003; Aldraihem and Khdeir, 2003), piezoelectric thin film mirrors that can be actively shaped using electric fields applied by an electron flux at selected locations (Martin et al., 2000; Martin and Main, 2002), and the post-cured shape of laminated composites (Hyer, 1981). Although these applications do not lie within the scope of this work, the approach that is developed can be readily applied to these and many other related problems.

Our proposed concept is to spatially vary eigenstrains within the layers of thin film microstructures by individually patterning the film layers. By spatially tailoring the eigenstrains, the shape of the microstructure can be controlled. We note that, in addition to generating the eigenstrains, the film patterns reinforce the structure, an effect working against the actuating eigenstrains. In order to control the shape, the key question that arises is how to pattern the film layers. In other words, where does one put the films, and what shape and size are the film patterns? The process of optimally determining the material distribution within a specified design domain, such that the resulting structure meets a set of design criteria, e.g., a prescribed deformational or *target* shape, is known as topology optimization. Topology optimization has been successfully applied to a wide range of structural and multi-physics design problems (Olhoff and Eschenauer, 1999; Bendsøe and Sigmund, 2003). However, topology optimization often yields complex shapes, which cannot be fabricated in a cost-effective manner using traditional fabrication processes. Therefore, topology optimization is often used as a conceptual design tool to obtain a sense of how to lay out material, and final designs are determined by squaring the optimal results heuristically with available manufacturing processes. Interestingly, this apparent shortcoming does not rear its head in the design of microsystems because geometrically complex structures are no more expensive to fabricate than simple ones due to the nature of thin-film fabrication technologies.

In the context of microsystems, topology optimization has been primarily applied to the design of two-dimensional mechanisms where actuation principles considered include piezoelectric, thermal, electro-thermal and electrostatic-mechanical coupling (Chen et al., 2001; Sigmund, 2001a,b; Moulton and Ananthasuresh, 2001; Yin and Ananthasuresh, 2002; Raulli and Maute, 2004). However, exploiting eigenstrains for out of plane actuation/deformation remains largely unexplored. Pedersen (2002) utilized thermal eigenstrains in the topological design of MEMS scale laminated microphone backplates optimized for both minimum compliance under a dead load and minimum predisplacement from the thermal prestress, which are essentially reinforcement problems. Reinforcement design via the independent patterning of layers in laminate plates or shells (Lee et al., 2000; Belblidia et al., 2001) differs from the actuator design of this work. Our intent is to utilize eigenstrains to generate large shape changes from an initially planar design rather than minimize the compliance of the structure by reinforcement, which is generally a small displacement problem.

In order to generate large shape changes via tailored eigenstrains, nonlinear geometric effects must be considered. These phenomena are rich and nontrivial. Over the years they have been studied for fully covered plates in various contexts including unsymmetric composite laminates (Hyer, 1981), thin-film technology for microelectronics applications (Masters and Salamon, 1993; Salamon and Masters, 1995; Finot and Suresh, 1996; Freund, 2000), and microsystems applications (Dunn et al., 2002; Zhang and Dunn, 2003, 2004). Numerous studies have considered geometrically nonlinear effects in structural topology

optimization (Bruns and Tortorelli, 2001; Buhl et al., 2000; Pedersen et al., 2001; Sigmund, 2001a,b; Maute and Frangopol, 2003). Recently, a fully nonlinear formulation for plate structures has been used by Kemmler (2004) to study the influence of geometrical instabilities on optimum layout.

In this paper, we develop a systematic approach to spatially tailor eigenstrains in multilayer thin-plate structures, including a geometrically nonlinear formulation into topology optimization. In Section 2 we describe the design approach, including the analysis of geometrically nonlinear multilayer structures, highlighting both the topology optimization process and the computational implementation. In Section 3 we briefly address the design of thin-film test structures, and the experimental techniques that are used to support the analysis and design efforts. Three interesting examples that demonstrate applications are presented in Section 4. Although they are necessarily focused on specific design problems, they highlight the generality of the approach. Concluding comments are made in Section 5.

2. Design approach

To generate locally varying eigenstrains which yield a desired deformation (target shape), the layout (location, size, shape) of patterns of the various layers is determined via topology optimization. The basic concept is illustrated in Fig. 2 in the context of a two-layer plate where the bottom layer is uniform (not patterned) and the top layer is patterned.

Our approach is general in that the design domain can contain an arbitrary number of layers, each of which can be arbitrarily patterned. In each layer the thermoelastic moduli are constant, but can be anisotropic in general. In our examples, we consider two- and three-layer structures where the layers are isotropic. Furthermore, in order to touch base with our experimental efforts, we consider the layers to be fabricated from gold and polysilicon. We keep the polysilicon layer uniform, and allow the gold layers to be patterned. Because of these specific choices we cast much of our discussion in terms of gold and polysilicon, but we remind that the approach is more general. The plate structure is discretized by a finite ele-

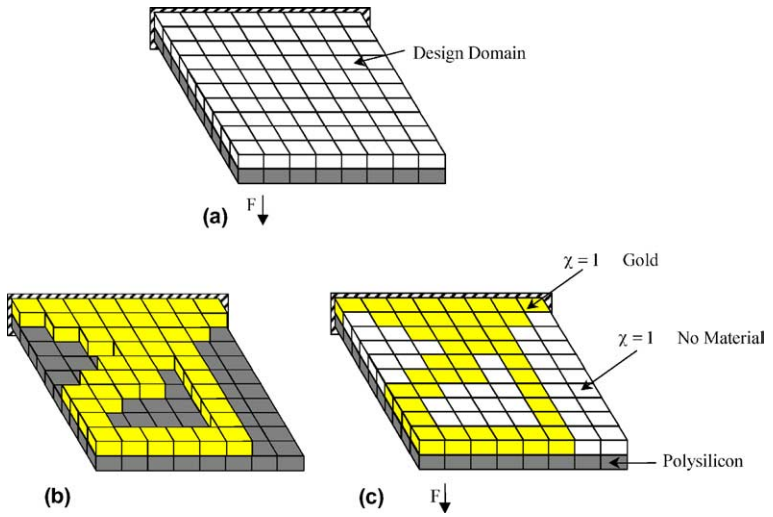

Fig. 2. Topology optimization for multilayer films with eigenstrains: (a) finite element discretization of design domain, (b) optimized material distribution in discretized domain, and (c) the finite element realization of the patterned layer in (b) where voids in the pattern are modeled as material with a negligible stiffness.

ment mesh with multilayer shell elements, and through the process of topology optimization, the patterns describing the layout of the gold layers are obtained.

2.1. Topology optimization

In order to determine the layout of the optimal pattern of the layers, one must formulate a design optimization problem that varies the distribution of one or multiple materials in a given design domain. This approach is commonly referred to as topology optimization, and the general approach is illustrated in Fig. 2. The geometry of a pattern is described by its material distribution, which in turn is defined by an integer-valued indicator function $\chi(\mathbf{x})$ in the design domain Ω. An arbitrary geometry can be described by $\chi(\mathbf{x})$, where $\chi(\mathbf{x}) = 1$ indicates that there is material and $\chi(\mathbf{x}) = 0$ indicates that there is no material at the point $\mathbf{x}$. In general, the material distribution problem is solved numerically by discretizing the design with finite elements, where the indicator function is assumed to take on a constant value over each element. As the resulting discretized integer problem is ill-posed, it leads to mesh-dependent results and is difficult to solve. The problem is relaxed by replacing the integer-valued indicator function with a continuously varying density function. The density in each element can vary between zero, that is no material, and ρ^0, which is the density of the bulk material. This smooth optimization problem can be efficiently solved by gradient-based optimizaton methods. As "0–1" material distributions are desired, tailored interplation schemes are used to relate material properties, such as the elastic modulus, to the variable density. These material interpolation schemes are most often nonphysical, but are computational vehicles to obtain "0–1" material distributions. In this work we employ the method known as simple isotropic material with penalization (SIMP, Bendsøe, 1989; Rozvany et al., 1992). The SIMP formulation may be understood as penalizing an intermediate material density by defining an effective material property, such as the Young's modulus E, to be a product of the bulk value and the density fraction raised to a power β:

$$E = E_0\left(\frac{\rho}{\rho_0}\right)^{\beta} = E_0(\chi)^{\beta} \tag{1}$$

where a β value of 3 has been used in this work to satisfy the Hashin–Shtrikman bounds on material properties (Bendsøe and Sigmund, 1999). Although the SIMP model was originally introduced for problems with mass constraints, with the intention of penalizing intermediate density values by suppling too little of the bulk property value for the associated mass, the concept has been applied to model many different material parameters (Sigmund and Torquanto, 1997; Bendsøe and Sigmund, 1999; Sigmund, 2001a). In this work, the Young's modulus is the only material property to be defined with the SIMP model. An optimized material distribution defined on the finite element discretization can be post-processed to obtain the optimum structural shape. This approach can be extended to incorporate multiple materials, as shown for example by Sigmund (2001b). As the results of the SIMP method alone are still mesh-dependent, a filtering scheme has also been employed in this work to ensure mesh independent results (Sigmund, 1994a,b).

The goal of the topology optimization problems considered here is to find the material distribution of the gold layer (denoted by a subscript 1) on a polysilicon layer such that the eigenstrains (here due to thermal expansion mismatch) cause a desired deformation. For example, an initially flat plate is deformed by a distribution of eigenstrains to achieve a target shape in the deformed configuration. This optimization problem can be written in general form as follows:

$$\begin{aligned} &\min_{\rho} \quad f(\boldsymbol{\rho}_1, \mathbf{u}(\boldsymbol{\rho}_1)) \\ &\text{s.t.} \quad g_j(\boldsymbol{\rho}_1, \mathbf{u}(\boldsymbol{\rho}_1)) \leqslant 0 \quad j = 1, \ldots, N_g \end{aligned} \tag{2}$$

where f is the objective and g_j denotes inequality constraints. The objective and constraints depend on the deformation and the material distribution of the gold, which is defined by the vector of density variables $\boldsymbol{\rho}_1$.

The components of $\boldsymbol{\rho}_1$ are the densities of the gold layer in each finite element. Evaluation of the objective and constraints takes place at the static equilibrium of the structure, which is attained by a standard finite element analysis of the structure at the current values of the material distribution. The general nature of the topology optimization problem formulation facilitates the use of general-purpose so-called "black-box" nonlinear optimization algorithms. In practice specialized algorithms tailored to accommodate the large number of optimization variables are used. In our approach, we use either the method of moving asymptotes (MMA, Svanberg, 1987) or a sequential quadratic program (SQP, Schittkowski, 1985; Gill et al., 1997).

As mentioned, the introduction of continuous density functions helps to solve the ill-posed nature of the integer-valued optimization problem. The smoothness introduced into the formulation facilitates the usage of gradient-based optimization algorithms, which require the gradients of the objective function and constraints with respect to density indicator variables known as sensitivities. For computational efficiency and accuracy reasons, we compute these gradient analytically by the adjoint method (Haug et al., 1986; Kleiber et al., 1997).

In the following discussion, the adjoint analytical sensitivity of the objective function f is derived, however the same derivation holds for any constraint g_j. The objective (and constraints) in this study may be expressed as a function of the nodal displacements $f(\mathbf{u})$. Because the structural response is a function of the continuous density indicator variables χ_i, the analytical gradients of the objective is therefore expressed

$$\frac{\mathrm{d}f}{\mathrm{d}\chi_i} = \frac{\partial f}{\partial \chi_i} + \frac{\partial f}{\partial \mathbf{u}} \frac{\mathrm{d}\mathbf{u}}{\mathrm{d}\chi_i} \tag{3}$$

where χ_i is the indicator variable corresponding to the ith element, and the explicit functional dependence of the objective function on the nodal displacements has been suppressed for clarity. Differentiation of the structural equilibrium residual equation with respect to the indicator function χ_i produces

$$\mathbf{K}\frac{\mathrm{d}\mathbf{u}}{\mathrm{d}\chi_i} = \frac{\partial \mathbf{f}_{\mathrm{ext}}}{\partial \chi_i} - \frac{\partial \mathbf{f}_{\mathrm{int}}}{\partial \chi_i} = \mathbf{P}_{\mathrm{A}} \tag{4}$$

where $\mathbf{K}$ is the tangent stiffness matrix, $\mathbf{f}_{\mathrm{int}}$ and $\mathbf{f}_{\mathrm{ext}}$ are the internal and applied structural forces, respectively, and $\mathbf{P}_{\mathrm{A}}$ is known as the pseudo-load vector. A combination of Eqs. (3) and (4) results in the expression for the adjoint sensitivity

$$\frac{\mathrm{d}f}{\mathrm{d}\chi_i} = \frac{\partial f}{\partial \chi_i} + \underbrace{\frac{\partial f}{\partial \mathbf{u}}\mathbf{K}^{-1}}_{\substack{\text{adjoint}\\ \text{response}}} \mathbf{P}_{\mathrm{A}} \tag{5}$$

The under-braced system in the above expression is a matrix-vector system that only requires solution once per criteria, per optimization iteration.

2.2. Multilayer thin plates with eigenstrains

We consider a multilayer elastic plate and within each material layer we permit an inelastic strain $\{\varepsilon^*\}$. The constitutive equation of the material in each layer is given by

$$\{\sigma\} = [E]\big(\{\varepsilon\} - \{\varepsilon^*\}\big) \tag{6}$$

In Eq. (6), $\{\sigma\}$ denotes the stress, $[E]$ the matrix of elastic moduli, and $\{\varepsilon\}$ the total strain. The source of this eigenstrain can be arbitrary; a common example is a thermal strain $\alpha\Delta T$ where α is the thermal expansion coefficient and ΔT a temperature change from some reference temperature. We model the deformation of such a layered plate using standard Kirchoff thin-plate kinematics. We recognize that these may lead to

inaccuracies due to thick-plate effects that exist locally near patterned features with characteristic in-plane dimensions on the order of the plate thickness, but numerical tests and measurements suggest that this approximation is reasonable in the description of the overall deformation behavior of the plate. In this work, we use three-node, 18-degree of freedom layered composite finite elements (Hemez, 1994) that consist of a combination of a membrane triangle with drilling degrees of freedom and an assumed quadratic rotation (AQR) bending triangle (Alvin et al., 1992; Felippa and Militello, 1992).

2.3. Co-rotational nonlinear finite element formulation

To account for large displacements, the co-rotational formulation is used (Nour-Omid and Rankin, 1991). It is a projector-based formulation that filters out the rigid body motion of a finite displacement, leaving only an elastic deformation. The resulting large displacement yet small strain element, in contrast to those derived from an updated or total Lagrangian formulation, utilizes a preexisting linear element, reducing the associated cost of implementation, especially if the linear element has a significant amount of existing analytical sensitivities. Our applications are large aspect ratio structures that undergo bending, justifying the usage of this large displacement, small strain model. Fig. 3 depicts the generalized description of motion of a co-rotational finite element deforming from its initial configuration to its final deformed configuration. The total deformation is broken down into two distinct motions: a rigid body motion from the initial configuration to the so-called shadow configuration, and a linear elastic deformation from the shadow configuration to the deformed configuration. Only the displacement from the shadow to the deformed configuration produces elastic deformation, and hence internal restoring force.

The elastic restoring force of an element is defined in the shadow configuration as

$$\mathbf{f}_{\text{elas}}^{(e)} = \mathbf{K}_{\text{ele}}^{(e)}\mathbf{v}_{\text{d}}^{(e)} \tag{7}$$

where $\mathbf{K}_{\text{ele}}^{(e)}$ is the stiffness matrix of a linear elastic element, $\mathbf{v}_{\text{d}}^{(e)}$ is the vector of elastic deformations, and the superscript (e) indicates a local element description. The expression for the elastic internal force in the global coordinate system is at the heart of the co-rotational formulation, and the resulting elemental expression is

$$\mathbf{f}_{\text{int}}^{(g)} = \mathbf{T}^{\text{T}}\mathbf{P}^{\text{T}}\mathbf{H}^{\text{T}}\mathbf{f}_{\text{elas}}^{(e)} \tag{8}$$

where $\mathbf{T}$ is the transformation matrix from the global to shadow configuration, $\mathbf{P}$ is the projector that filters out the contributions of rigid body motions, and $\mathbf{H}$ is a matrix which relates the instantaneous deformational rotational degrees of freedom used in the iterative nonlinear equilibrium analysis to the finite visible rotational degrees of freedom.

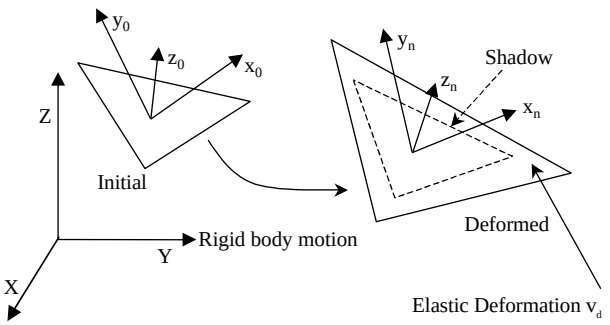

Fig. 3. Illustration of the co-rotational concept.

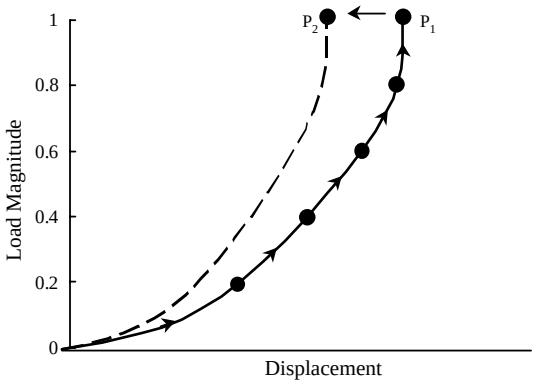

Fig. 4. Illustration of the restart procedure used in the load-controlled incremental Newton–Raphson algorithm.

If an external force term is dependent on the structural displacements, for example the forces generated from hydrostatic pressure, then these external forces are expressed in global coordinates as

$$\mathbf{f}_{\text{ext}}^{(\text{g})} = \mathbf{T}^{\text{T}}\mathbf{H}^{\text{T}}\mathbf{f}_{\text{ext}}^{(\text{e})} \tag{9}$$

where $\mathbf{f}_{\text{ext}}^{(\text{e})}$ is the external force acting on the corresponding linear finite element expressed in local coordinates. The projector term has been left off this expression of the external force because no portion of the applied force should be projected out. These expressions of the internal and external forces are used in the definition of the residual equation, which is solved using a load-controlled Newton–Raphson algorithm. The linearization of the residual definition results in the expression for the tangent stiffness matrix, which may become unsymmetric when the elements exhibit bending deformations.

In order to reduce the solution time associated with the incremental nonlinear analysis, each successive equilibrium analysis is started from the point of the previously converged solution. This idea is shown in the load–deflection curves of Fig. 4. After converging to point P_1 using a fractional load increment in the first analysis, step 2 is begun from point P_1 and the full load is applied to get to point P_2. This process is then repeated in each subsequent step. This method is more expedient than beginning again from the undeformed configuration and applying the load in incremental steps again to reach P_2. An issue that often arises in finite element analysis with topology optimization is the removal of so-called void nodes (nodes surrounded by low-density material) from the residual convergence criteria (Buhl et al., 2000; Pedersen et al., 2001). This is unnecessary for our problems because low-density regions in the computational mesh do not occur as the substrate onto which materials are deposited is always present, which provides sufficient stiffness to remove oscillations in low-density regions.

3. Experimental support

In order to validate the analysis and optimization procedures, at least to some degree, we fabricated thin-film microstructures consistent with predicted optimal topologies, and measured full-field displacements and curvature developed when they were subject to a uniform temperature change. The thin-film plates were fabricated with two film layers, polycrystalline silicon (polysilicon) and gold. The polysilicon film is a continuous plate of either 1.5 μm or 3.5 μm thickness, and the 0.5 μm thick gold film is patterned on top of the polysilicon. The plates were fabricated using the commercially available Multi-User MEMS Process (MUMPs, Koester et al., 2001). This so-called surface micromachining process consists of a series of standard microelectronics lithography, thin-film deposition, and etching processes, and is described in de-

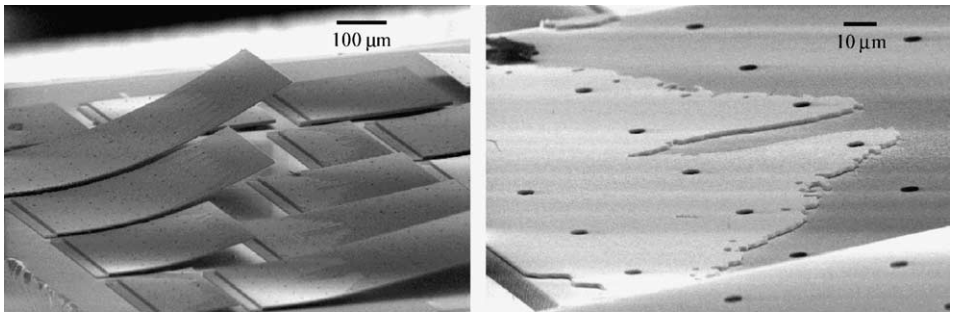

Fig. 5. Left: Scanning electron micrographs of plate microstructures manufactured from the optimal designs associated with the applications in Section 4.1. Right: The plates consist of a gold layer patterned onto a polysilicon substrate.

tail elsewhere (Zhang and Dunn, 2004). The final result is a thin-film microstructure that is released from the substrate; except for its supports, it is free. Scanning electron micrographs of typical microstructures are shown in Fig. 5.

After release from the substrate, the plates are thermal cycled three times between room temperature and 190 °C to try to stabilize the gold material microstructure since it is well-known that significant microstructural evolution can occur during the first thermal cycle after deposition (Nix, 1989; Baker et al., 2001; Zhang and Dunn, 2003). After the initial thermal cycles, the microstructures are heated to 100 °C at a rate of 10 °C/min, and then cooled at the same rate. The deformation during cooling is then due to linear and geometrically nonlinear thermoelasticity.

We measured the full field out of plane displacement of the microstructures as a function of temperature change with scanning white light interferometry using an interferometric microscope and a custom-built temperature chamber. The resolution of the out of plane displacement measurements, $w(x,y)$, is at least 5 nm as verified by making measurements on standards, the resolution of the temperature chamber is about 1 °C and the lateral spatial resolution is about 2.7 μm. In order to determine curvature we fit the measured displacement field with a polynomial function of position and then differentiated the polynomial in the standard manner.

In order to validate both linear and geometrically nonlinear analysis capabilities, we also fabricated a freestanding circular gold/polysilicon plate and measured the full-field displacements during cooling. Fig. 6 contains contour plots of the measured and predicted displacement field $w(x,y)$ at room temperature for circular plates of three different diameters: $D = 150$, 200, and 250 μm. Due to the thermal expansion mismatch between the polysilicon and gold, the plates deform in a spherically symmetric manner; contours of constant out of plane displacement $w(x,y)$ are nearly circles. Both the measured and nonlinear response predicted $w(x,y)$ contours show this behavior and the agreement between them is quite good.

Fig. 7 shows the average curvature in the radial direction as a function of the magnitude of the temperature change during cooling. The temperature change is actually negative, that is a temperature decrease, but its magnitude is plotted for convenience throughout the paper. Both the measurements and predictions show two regimes of deformation: in regime I (a temperature change less than about 20 °C), the curvature–temperature response is linear and independent of plate size and shape. In regime II (a temperature change greater than about 20 °C), though, the behavior is nonlinear, and there is a strong dependence on plate size. This dependence on plate size and deformation (increased temperature leads to increased deformation) indicates that the nonlinear behavior is geometric in nature. Good agreement exists between the measurements and predictions in both deformation regimes. These results demonstrate the ability of the analysis capabilities, a necessity for its use for topology optimization. More extensive studies of the deformation of different size and shape plates, including a third deformation regime, buckling, can be found in Dunn et al. (2002).

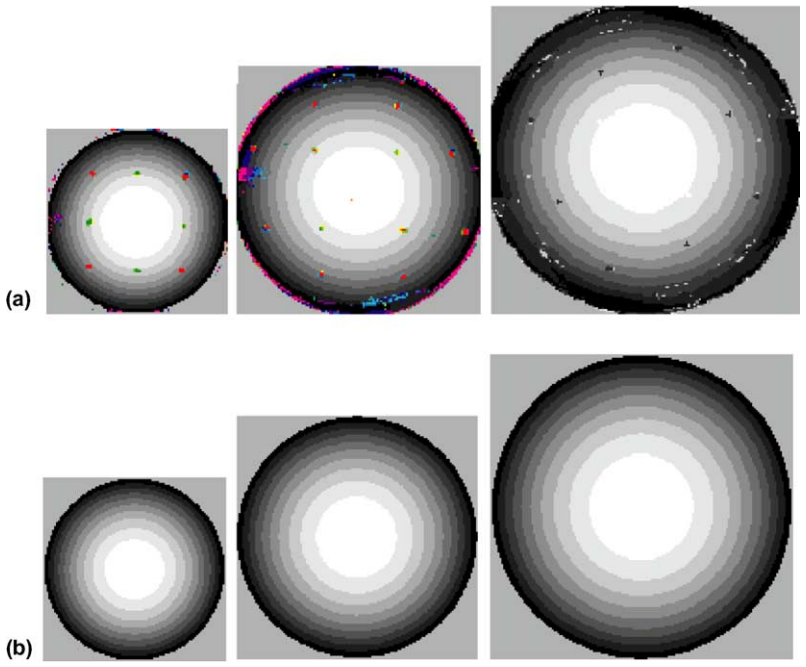

Fig. 6. Contour plots of the (a) measured, and (b) predicted (nonlinear), out of plane displacements $w(x, y)$ at room temperature after cooling from 100 °C for the three gold/polysilicon circular plates: $D = 150$, 200, and 250 μm from left to right. Each contour band represents a displacement of 0.13, 0.22, and 0.29 μm for the $D = 150$, 200, and 250 μm plates, respectively.

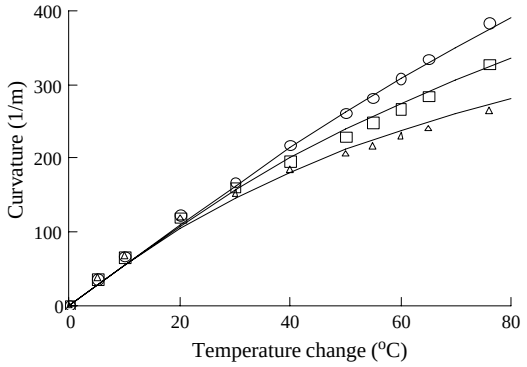

Fig. 7. Average measured (symbols) and nonlinear response predicted (curves) curvature as a function of temperature change upon cooling from 100 °C to room temperature. The curves and symbols from top to bottom are for the circular plates $D = 150$, 200, and 250 μm structures, respectively.

4. Applications

We applied our approach to three interesting examples that demonstrate the capabilities of the methodology. The first two are cantilevered plates that are motivated by applications in microfluidic mixing. The third application demonstrates the ability to use eigenstrains to achieve twisting deformation. In each case the design domains of the topology optimization problem span the gold deposition layer or layers; the poly-

Table 1
Material properties used in the applications section

Material	E [GPa]	ν	α [K^{-1}]
Gold	78	0.42	14.4
Polysilicon	163	0.22	2.8

silicon layer in each problem is nonvariable and assumed to span the domain specified in each example. The application of gold layer(s) to the polysilicon produces two competing phenomena. It both increases the stiffness (reinforcement) and produces the eigenstrains required for the out of plane deformation (actuation). It is worth noting here that these problems do not require mass constraints, typically needed in topology optimization, in order to obtain a clear "0–1" material distribution. This fortuitous situation is a result of the formulation of the optimization problems. Traditionally, the topology optimization of compliant mechanisms requires a spring at the output port, e.g., the point on the structure where the displacements are to be maximized, in order to avoid intermediate material densities that do not transfer forces effectively throughout the structure. The presence of a polysilicon film layer that spans the structure acts as an effective spring at every point in the structure. The material properties for gold and polysilicon are given in Table 1.

4.1. Cantilevered plate with a flat end

One method of microfluidic mixing entails the use of electrostatically actuated flaps to introduce turbulence into the flow. Ma et al. (2003) created microfans that consist of electrostatically actuated plates that drive fluid flow in resonance. Ideally these plates would exhibit cylindrical curvature, but the creation of curvature through eigenstrains in blanketed bilayer films results in undesirable biaxial curvature. A viable approach to the realization of curved microflaps is to use multilayer thin films and their associated eigenstrains, e.g., thermal expansion mismatch when subjected to a uniform temperature change, as long as the curvature inherent in these devices is controlled to produce desirable actuated shapes.

We consider a design domain consisting of a plate, with side lengths L and W, cantilevered along one edge shown in Fig. 8. The plate consists of two layers, a 1.5 μm thick bottom layer of polysilicon and a 0.5 μm thick top layer of gold, and is subjected to a 75 °C temperature decrease from the temperature that the plate lies flat, about 100 °C in practice. If the gold layer completely covers the polysilicon layer, the edge opposite the cantilevered side raises upwards, but it will not be flat. Instead, the edge will exhibit curvature along the direction orthogonal to the lift. We attempt to design a structure where the gold layer is patterned in such a way that the displacement of the raised edge is maximized while the transverse curvature is eliminated.

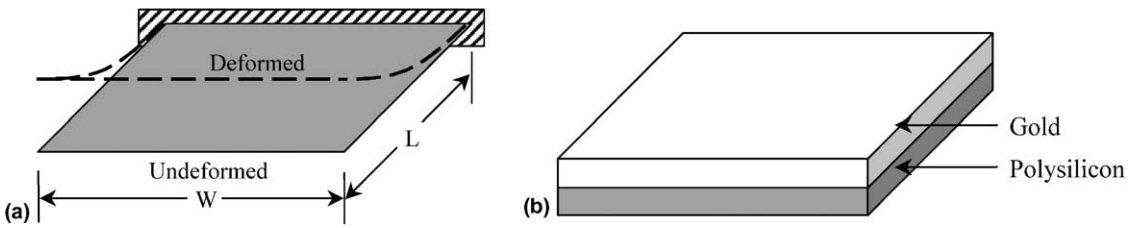

Fig. 8. Diagram of the cantilevered plate with a flat edge problem. The structure is shown in (a) along with a visualization of liftoff to be maximized by patterning gold onto the layer above the polysilicon, as seen in (b).

To this end we formulate an optimization problem as

$$\begin{aligned} &\max \quad d \\ &g_1 = \sum_{i=1}^{n} (w_i - d)^2 \leqslant \varepsilon^2 \end{aligned} \tag{10}$$

where w_i is the vertical displacement at the ith of n equispaced nodes along the raised edge, and d is the average nodal displacement along the raised edge defined as

$$d = \frac{1}{n} \sum_{i=1}^{n} w_i \tag{11}$$

In this example, $n = 7$ and the prescribed tolerance $\varepsilon = 0.1$ μm. The examples in the subsection use a mesh of 30×30 rectangular elements (derived from four overlapping triangular elements), resulting in 900 optimization variables to mesh half of the symmetric design domain.

To provide a baseline with regard to the behavior of the optimum plates, Fig. 9 contains comparisons of measurements and predictions for a $L = W = 300$ μm plate cantilevered along one edge that is fully covered with gold. The average measured and predicted curvature versus temperature change along both the center of the plate from the fixed to the cantilevered end and the across the free edge are shown. Clearly significant transverse curvature results when the plate is fully covered. In the optimum designs the curvature along the free end will be reduced to nearly zero.

In addition to a square plate of $L = W = 300$ μm, two additional variations on this topology optimization problem have been considered: doubling the length of the cantilevered plate ($L = 600$ μm, $W = 300$ μm), and increasing the polysilicon layer thickness to 3.5 μm ($L = W = 300$ μm). The resulting gold pattern topologies considering both linear and nonlinear structural response are shown in Figs. 10–12 for the square design, double length design, and increased polysilicon thickness design, respectively. Fig. 5 displays several optimal plate designs in the deformed configurations.

The optimal gold patterns that produce flat raised edges contain similar characteristics, regardless of the plate size or polysilicon layer thickness; the gold is patterned beginning at the base of the supported end and extends outwards. With the exception of the 3.5 μm thick polysilicon case, significant differences do exist between optimal designs obtained with linear and nonlinear mechanics. The gold patterns of nonlinear structure solutions extend out further from the support, and do not contain a recessed region in the center as their linear response counterparts do. Both of these characteristics are a result of geometrically nonlinear

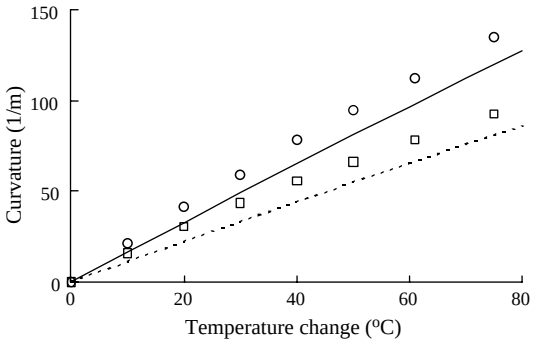

Fig. 9. Average measured and predicted curvature as a function of temperature change upon cooling from 100 °C to room temperature for $W = L = 300$ μm gold (0.5 μm thick)/polysilicon (3.5 μm thick) cantilevered plates. Solid line and (○) indicate average predicted and measured curvature along the length of the plate; dashed line and (□) indicate average predicted and measured curvature across the tip.

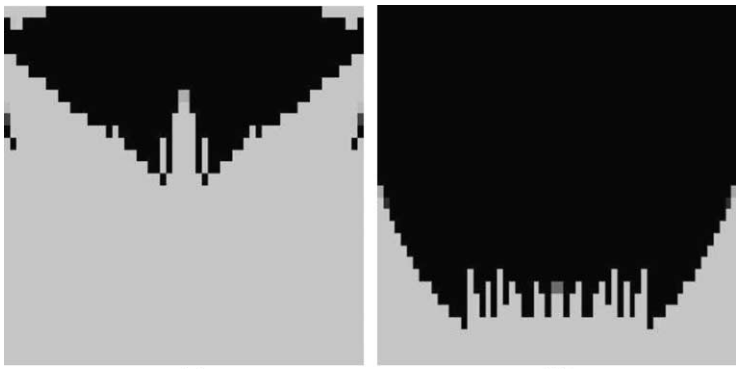

Fig. 10. Optimal topologies of $L = W = 300$ μm cantilevered plate with a 1.5 μm thick polysilicon layer obtained considering a linear (a) and nonlinear (b) structural response. Black indicates the 0.5 μm thick gold deposition pattern; the upper edge is cantilevered.

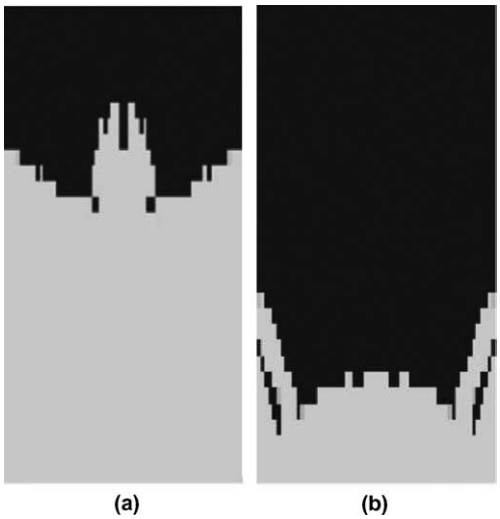

Fig. 11. Optimal topologies of $L = 600$ μm, $W = 300$ μm cantilevered plate with a 1.5 μm thick polysilicon layer obtained considering a linear (a) and nonlinear (b) structural response. Black indicates the 0.5 μm thick gold deposition pattern; the upper edge is cantilevered.

plates becoming stiffer in bending than the linear counterparts. The gold patterns can extend further from the cantilevered base without significantly increasing the curvature along the raised edge. To exclude the possibility of local minima, it is noted that optimization with a linear structural response starting from the design optimized using a nonlinear kinematics produces the linear response design presented here. This is also conversely true regarding the optimum design for the nonlinear kinematics. Fig. 13 shows predicted contour plots for the cantilevered gold/polysilicon plates for the presented cases. The contour plots are for fully covered linear, nonlinear, optimized linear, and optimized nonlinear plates from left to right, respectively. A comparison of the linear and nonlinear fully covered plate displacement profiles indicates the reduction in transverse curvature inherent in the nonlinear plate bending mechanics. The displacement profiles of the fully covered and optimal plates clearly show the reduction of curvature present in both the linear and nonlinear optimal cases.

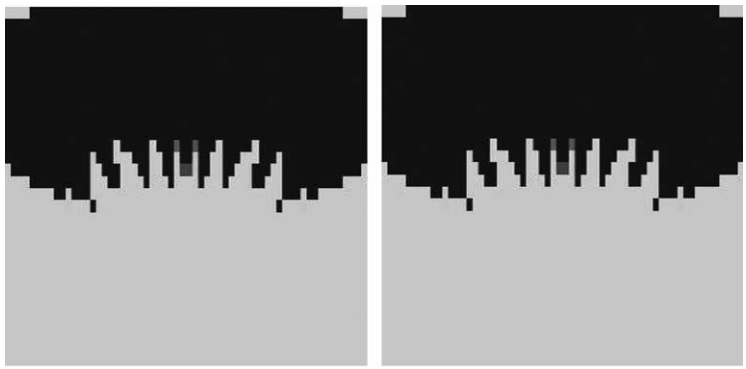

Fig. 12. Optimal topologies of $L = W = 300$ μm cantilevered plate with a 3.5 μm thick polysilicon layer obtained considering a linear (a) and nonlinear (b) structural response. Black indicates the 0.5 μm thick gold deposition pattern; the upper edge is cantilevered.

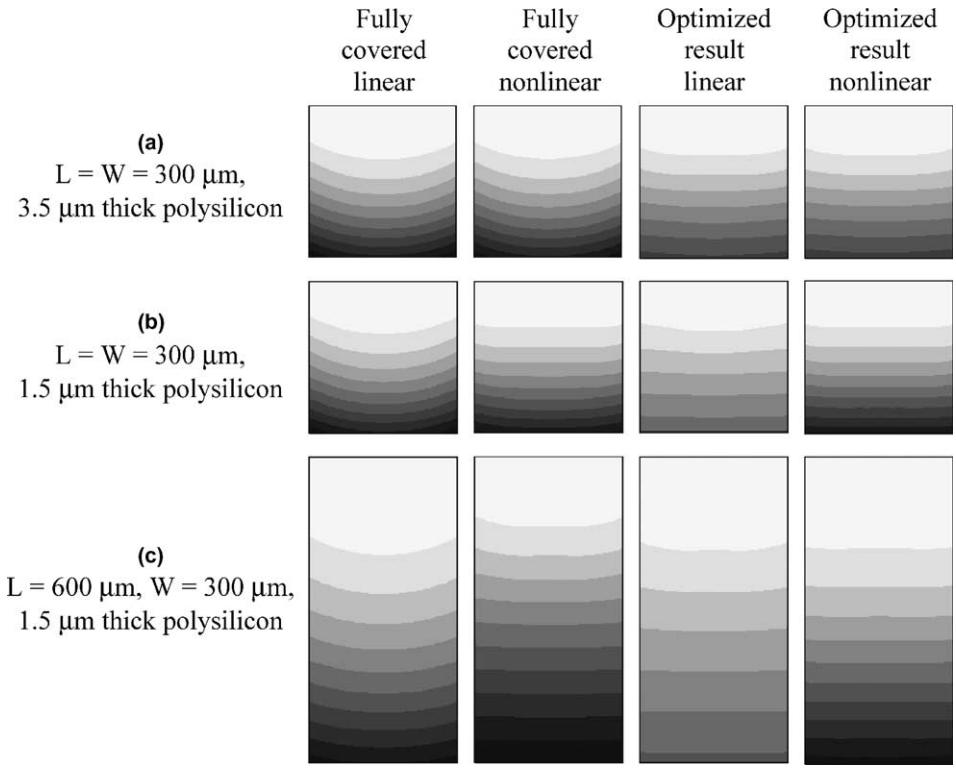

Fig. 13. Predicted contour plots for gold (0.5 μm thick)/polysilicon cantilevered plates for various dimensions; (a) each contour band represents 0.7 μm; (b) each contour band represents 2.45 μm; (c) each contour band represents 8.94 μm.

In addition to the visual difference between the optimal solutions using linear and nonlinear kinematics, the numerical differences are significant. Table 2 displays the resulting vertical liftoff of the flat edge for the various plate sizes and layer thicknesses. A nonlinear structural analysis of the $L = W = 300$ μm plate optimal topology obtained using a linear kinematics (seen in Fig. 10a) shows slight curvature along the raised

Table 2
Resulting objectives d (vertical displacement) and constraints g_1 for a linear or nonlinear analysis of the optimal designs of the cantilevered plate with a flat edge problem obtained using a linear or nonlinear structural response

Flat edge plate dimensions	Linear analysis linear optimum	Nonlinear analysis nonlinear optimum	Nonlinear analysis linear optimum
$L = 300$ μm, $W = 300$ μm 0.5 μm gold/1.5 μm polysilicon	$d = 12.1$ μm $g_1 = 0.01$ μm^2	$d = 21.7$ μm $g_1 = 0.01$ μm^2	$d = 13.0$ μm $g_1 = 0.0169$ μm^2
$L = 600$ μm, $W = 300$ μm 0.5 μm gold/1.5 μm polysilicon	$d = 51.0$ μm $g_1 = 0.01$ μm^2	$d = 85.0$ μm $g_1 = 0.01$ μm^2	$d = 51.3$ μm $g_1 = 0.0004$ μm^2
$L = 300$ μm, $W = 300$ μm 0.5 μm gold/3.5 μm polysilicon	$d = 4.1$ μm $g_1 = 0.01$ μm^2	$d = 4.1$ μm $g_1 = 0.01$ μm^2	$d = 4.1$ μm $g_1 = 0.01$ μm^2

Note that the constraints are identically satisfied in most cases.

edge, $g_1 = 0.0169$ μm^2, despite a similar objective value $d = 13.0$ μm. This highlights the need for a geometrically nonlinear analysis to obtain truly optimal solutions. Fig. 14 shows measured and predicted surface profiles along the raised free edge for the gold/polysilicon (1.5 μm thick polysilicon) plates optimized with a nonlinear response. The measurements and predictions are in good agreement. At first glance this might not appear to be the case for the plate in Fig. 14b as the measurement shows a downward curvature in contrast to the predicted upward curvature. However, the deflections, both measured and predicted, are so small that this difference is insignificant, especially when compared to the total tip deflection (relative to the fixed end) of 85 μm.

Fig. 15 shows the measured and predicted surface profiles along the free edge for the $L = W = 300$ μm plate (3.5 μm thick polysilicon) optimized with a nonlinear response. Excellent agreement is observed. Again the variation in deflection across the free end is quite small, by design. The resulting optimal gold deposition patterns for the square plate with an increased polysilicon thickness are the same for both the linear and nonlinear mechanics. The thicker polysilicon layer greatly increases the plate stiffness, reducing the displacements, and rendering the problem linear. The lack of a necessity for including a geometrically nonlinear response in this problem is evident, however it is worth noting that one cannot justify this until the solutions obtained with linear and nonlinear kinematics are shown to be equivalent.

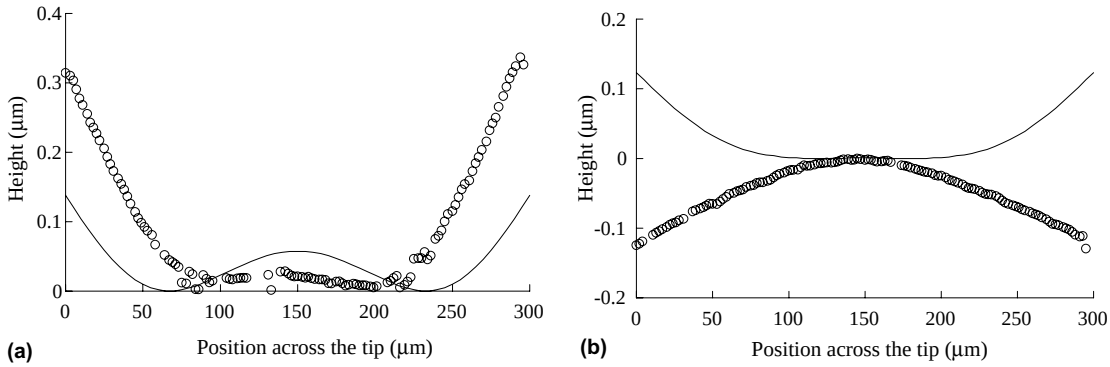

Fig. 14. Measured and predicted surface profile along the free end for the gold (0.5 μm thick)/polysilicon (1.5 μm thick) plates with nonlinear optimization: (a) $L = W = 300$ μm, (b) $L = 600$ μm, $W = 300$ μm. The average displacement of the free end for each case is 21.7 μm for (a) and 85.0 μm for (b).

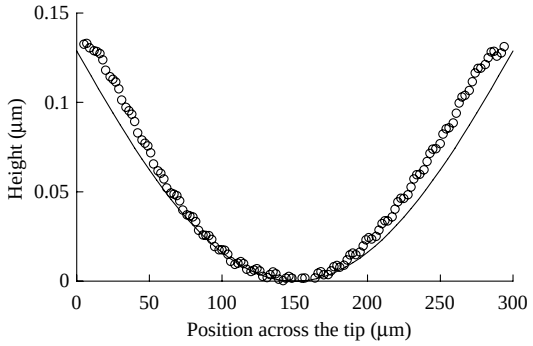

Fig. 15. Measured and predicted surface profile along the free end for the gold (0.5 μm thick)/polysilicon (3.5 μm thick) $L = W = 300$ μm plate with nonlinear optimization. The average displacement of the free end is 4.1 μm.

4.2. Cantilevered plate with a curved end

Although the flat edge in the previous example is an appropriate design goal, especially for the microfluidic mixing problem, our approach is not limited to any specific shape of the raised edge, or to any part of the structure for that matter. The open-ended nature of the optimization problem formulation allows one to enforce any constraint, with a flat raised edge being only one of an infinite number of possibilities. To illustrate this point, we revisit the $L = W = 300$ μm plate problem of the preceding subsection. The goal now, however, is to maximize the average liftoff of the raised edge, while making the edge adopt a negative curvature (curvature opposite to that of the lift). To create this doubly curved design, a third layer must be introduced to the cantilevered plate. We allow for a top and bottom layer of gold (0.5 μm thick) to be patterned arbitrarily as they sandwich a complete polysilicon layer (1.5 μm thick). Again a 75 °C temperature decrease is imposed on the structure shown in Fig. 16.

We formulate the optimization problem as

$$\begin{aligned} \max \quad & d \\ & g_1 = \kappa \leqslant \varepsilon \end{aligned} \tag{12}$$

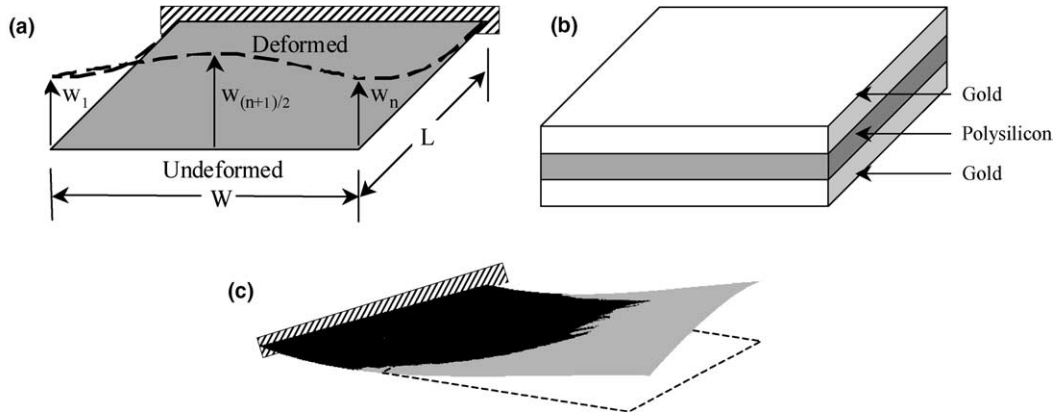

Fig. 16. Diagram of cantilevered plate with a curved edge problem. The structure is shown in (a) with a visualization of the liftoff to be maximized by patterning gold into the layers above and below the polysilicon layer, seen in (b). Note the doubly curved surface in (a). The computer generated deformation shown in (c) is the optimal solution obtained using a nonlinear kinematics.

where d is the average displacement along the raised edge as defined as in Eq. (11) with $n = 9$, ε is a specified curvature constraint, and κ is the curvature across the free edge:

$$\kappa = \left(\frac{2}{L}\right)^2 (w_1 - 2w_{(n+1)/2} + w_n) \tag{13}$$

In Eq. (13), L is the length of the plate along the free edge, w_1 and w_n are the vertical displacements of the nodes at the free corners, and $w_{(n+1)/2}$ is the vertical displacement of the center node along the free edge. The meshes used in the examples of this subsection consist of 6.25 μm × 6.25 μm square elements, resulting in 4608 optimization variables. The resulting topologies for an enforced curvature of $\varepsilon = -178\ \mathrm{m}^{-1}$, using both a linear and nonlinear structural response, are shown in Figs. 17 and 18, respectively. Fig. 16c displays the computer generated deformed configuration for the optimal solution obtained with nonlinear mechanics.

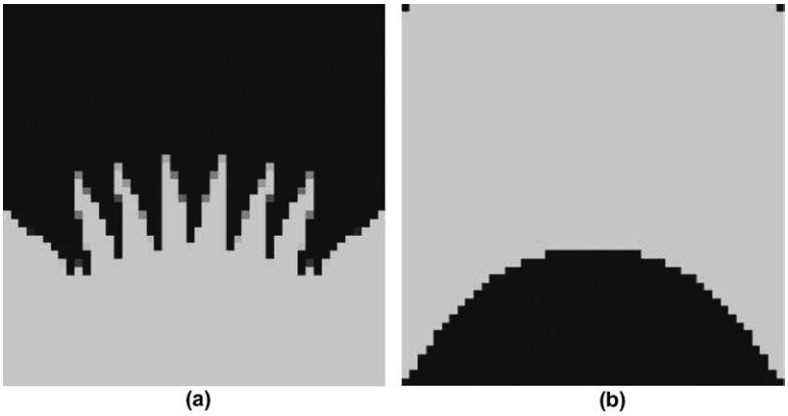

Fig. 17. Optimal topologies of $L = W = 300$ μm cantilevered plate with a 1.5 μm thick polysilicon layer exhibiting negative curvature $\kappa = -178\ \mathrm{m}^{-1}$ obtained considering a linear structural response. Black indicates the 0.5 μm thick gold deposition pattern of the top (a) and bottom (b) gold layers; the upper edge is cantilevered.

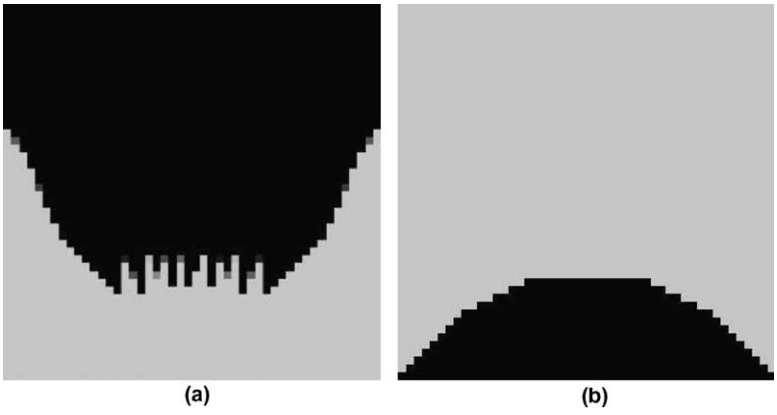

Fig. 18. Optimal topologies of $L = W = 300$ μm cantilevered plate with a 1.5 μm thick polysilicon layer exhibiting negative curvature $\kappa = -178\ \mathrm{m}^{-1}$ obtained considering a nonlinear structural response. Black indicates the 0.5 μm thick gold deposition pattern of the top (a) and bottom (b) gold layers; the upper edge is cantilevered.

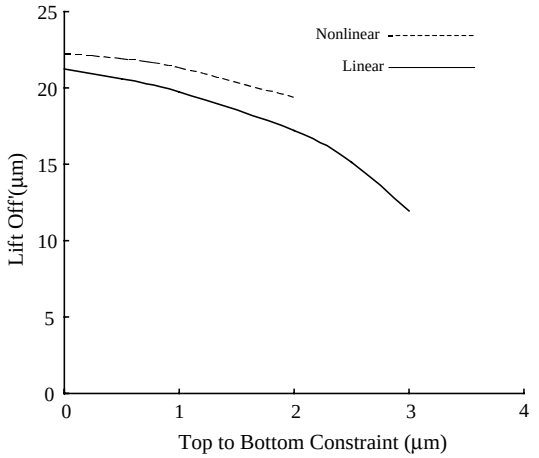

Fig. 19. Relationship between objective (mean vertical displacement of the raised edge) and imposed constraint for the negative curvature plate problems. Results obtained considering a linear structural response allow for a larger constraint to be imposed. Note that here the top to bottom constraint is expressed $c = w_{(n+1)/2} - w_1$.

The gold patterns that lead to negative curvature along the raised edge of the square plate invoke similar mechanics principles as those used to keep the raised edge flat. The top layer of gold extending out from the cantilever support provides the bending mechanism required to lift the opposite edge upwards. On the lower gold layer, the gold is patterned near the raised edge to induce the prescribed negative curvature. Fig. 19 displays the relationship between the mean vertical displacement of the raised edge and the crest to trough displacement along this edge. The trends are intuitive; increasing the prescribed negative curvature results in a decreasing vertical liftoff. It is noteworthy that the optimization approach cannot find suitable designs for a nonlinear structural response when the negative curvature constraint becomes too demanding. The nonlinear plate is stiffer than its linear counterpart in the bending direction orthogonal to the primary out of plane lift, making designs with the desired curvature infeasible. This example serves to highlight another benefit of using geometrically nonlinear analysis in the topology optimization process: the prevention of unrealizable designs.

Although actual fabrication would require a more involved process than that discussed in Section 3, the use of a bottom gold layer allows for an increase in the vertical displacement of a flat raised edge like that in Section 4.1 (0 valued constraint in Fig. 19). The inclusion of this extra layer results in a design that outperforms the two-layer design that only contains a single upper layer of gold. This occurs because the lower gold layer operates as a correction for too much upward curvature that occurs from increasing the objective by placing more gold on the upper surface.

4.3. Twist strip

In addition to manipulating eigenstrains in multi-layered thin films to produce bending deformations, our approach can also be used to yield thin-film structures that twist, or for that matter exhibit prescribed combinations of flexure, twist, and extension/contraction. Fig. 20 shows a schematic of a design problem that illustrates the ability to twist. The design domain consists of a 200 μm × 50 μm area with a 50 μm × 20 μm gap notched out along the cantilevered edge. We intend to determine the patterns of 0.5 μm thick gold films both on top of and below a 0.5 μm thick layer of polysilicon film, so that the resulting eigenstrains (thermal strains between the layers from a 300 °C temperature increase) will maximize the twist along the long axis of the structure. The mesh used contains 2.5 μm × 2.5 μm square elements, result-

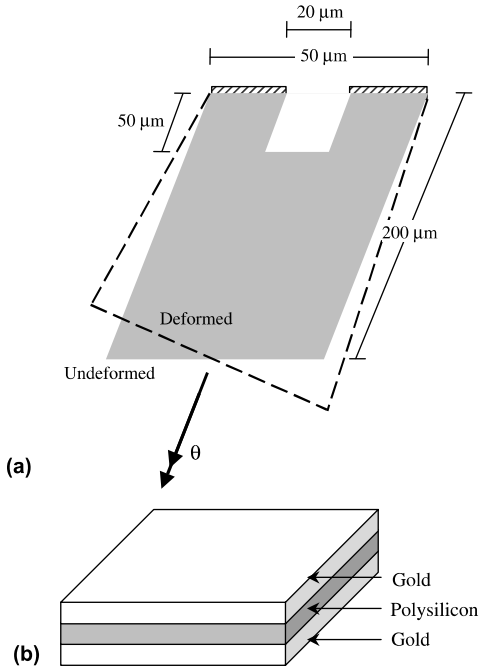

Fig. 20. Diagram of screwdriver strip problem. The polysilicon base layer is shown in (a) along the a visualization of the rotation to be maximized by patterning gold into the layers above and below the polysilicon layer, seen in (b).

ing in 3040 optimization variables. The resulting gold patterns and deformed shapes when considering both a linear and nonlinear structural response are shown in Fig. 21.

The topologies of the gold patterns for the twisting plate problem display the same basic patterns for the linear and nonlinear structural results. The anti-symmetry between the top and bottom layers is immediately evident, and plays a central role in the twisting mechanism. The gold patterns located adjacent to the notch near the cantilevered edge on the top/bottom layer provide the basic lowering/lifting mechanism

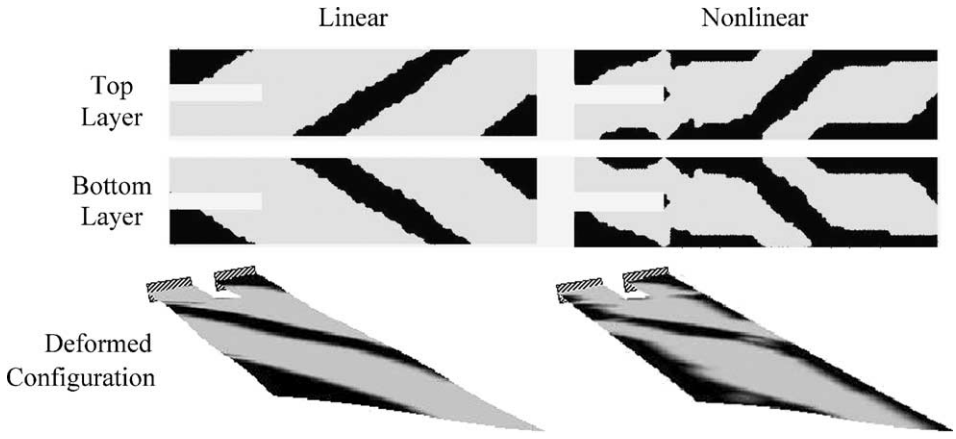

Fig. 21. Optimal topologies and deformed shapes for the screwdriver strip problem obtained considering a linear (left) and nonlinear (right) structural response. Black indicates the gold deposition pattern on the upper and lower gold layers. The left edge is cantilevered.

responsible for the twisting motion. This motion is further increased by both the crossed pattern appearing along the length of the mechanism and the gold patterns located at the twisted end. The similarity with a $\pm 45^\circ$ composite laminate, which is well known to produce twist, is evident. The rotation angles achieved for the optimal linear and nonlinear response designs are 27.6° and 25.6°, respectively. Optimization with linear response appears to outperform the result achieved with nonlinear mechanics, however a geometrically nonlinear analysis of the optimal linear kinematics design results in a twist angle of only 20.2°. This indicates that this problem is not within the regime of a linear mechanics model, and that a geometrically nonlinear analysis is required to accurately model the physical phenomena.

5. Summary and conclusions

Although many microsystem fabrication technologies are based on planar thin film technologies, eigenstrains, for example those arising from thermal expansion mismatch between layers, may be manipulated to deform a planar structure into one with a three-dimensional shape. We developed a methodology for the design of such multilayer thin films by topology optimization. We have shown that it in many cases it is necessary to incorporate the effects of geometric nonlinearity, both to obtain optimal objective values, and also to avoid physically unrealizable designs. We applied our methodology to the design of microfluidic mixing flaps, and a microscrewdriver-like mechanism. The flaps demonstrate the ability to control curvature of plate-like structures, primarily due to bending. This includes the possibility of curvature that is positive in one direction and negative in the other. The screwdriver-like mechanism demonstrates the ability to design structures with twist curvature. We fabricated a series of optimal microstructures with gold and polysilicon layers, and measured the deformed shapes when subjected to the prescribed eigenstrains, via thermal expansion mismatch between the layers when subjected to a uniform temperature change. Good agreement was achieved between predicted shapes and those measured using white-light interferometry. The design methodology can be used to yield plate-like structures with shapes that result from a one-time imposition of the eigenstrains, or ones that can be repeatedly actuated by the repeated application of the eigenstrains. Although we developed and presented our approach in the context of the design of three-dimensional microstructures, it can be easily applied to a variety of diverse problems where it is desired to control the complex shape and/or output force characteristics of plate-like structures by actuation mechanisms that are spatially distributed, and the actuators are represented by potentially anisotropic eigenstrains.

Acknowledgements

The first two authors acknowledge the support by the National Science Foundation under grant DMI-0300539 and DMI-0348759. All authors acknowledge the support through the Air Force Office of Scientific Research under grant F49620-02-1-0037. The opinions and conclusions presented are those of the authors and do not necessarily reflect the views of the sponsoring organizations.

References

Aldraihem, O.J., Khdeir, A.A., 2003. Precise deflection analysis of beams with piezoelectric patches. Composite Structures 60, 135–143.

Alvin, K., de la Fuente, H.M., Haugen, B., Felippa, C.A., 1992. Membrane triangles with corner drilling freedoms—I. The EEF element. Finite Elements in Analysis and Design 12, 163–187.

Baker, S.P., Kretschmann, A., Arzt, E., 2001. Thermomechanical behavior of different texture components in Cu thin films. Acta Materialia 49, 2145–2160.

Belblidia, F., Lee, J.E.B., Rechak, S., Hinton, E., 2001. Topology optimization of plate structures using a single- or three-layered artificial material model. Advances in Engineering Software 32, 159–168.

Bendsøe, M.P., 1989. Optimal shape design as material distribution problem. Structural Optimization 1, 193–202.

Bendsøe, M.P., Sigmund, O., 1999. Material schemes in topology optimization. Archive of Applied Mechanics 69, 635–654.

Bendsøe, M.P., Sigmund, O., 2003. Topology Optimization: Theory, Methods and Applications. Springer.

Brittain, S.T., Sugimura, Y., Schueller, O.J.A., Evans, A.G., Whitesides, G.M., 2001. Fabrication and mechanical performance of a mesoscale space-filling truss system. Journal of Microelectromechanical Systems 10, 113–120.

Bruns, T.E., Tortorelli, D.A., 2001. Topology optimization of nonlinear elastic structures and compliant mechanisms. Computer Methods in Applied Mechanics and Engineering 190, 3443–3459.

Buhl, T., Pedersen, C.B.W., Sigmund, O., 2000. Stiffness design of geometrically nonlinear structures using topology optimization. Structural and Multidisciplinary Optimization 19, 93–104.

Chen, B.C., Silva, E.C.N., Kikuchi, N., 2001. Advances in computational design and optimization with applications to MEMS. International Journal for Numerical Methods in Engineering 52, 23–62.

Dunn, M.L., Zhang, Y., Bright, V.M., 2002. Deformation and structural stability of layered plate microstructures subjected to thermal loading. Journal of Microelectromechanical Systems 11, 372–384.

Felippa, C.A., Militello, C., 1992. Membrane triangles with corner drilling freedoms—II. The ANDES element. Finite Elements in Analysis and Design 12, 189–201.

Finot, M., Suresh, S., 1996. Small and large deformation of thick and thin film multilayers: effects of layer geometry, plasticity and compositional gradients. Journal of the Mechanics and Physics and Solids 44, 683–721.

Freund, L.B., 2000. Substrate curvature due to thin film mismatch strain in the nonlinear deformation range. Journal of the Mechanics and Physics and Solids 48, 1159–1174.

Gill, P.E., Murray, W., Saunders, M.A., 1997. SNOPT: an SQP algorithm for large-scale constrained optimization. In: Report NA 97-2, Department of Mathematics, University of California, San Diego.

Harsh, K.F., Bright, V.M., Lee, Y.C., 1999. Solder self-assembly for three-dimensional microelectromechanical systems. Sensors and Actuators A 77, 237–244.

Haug, E.J., Choi, H.K., Komlov, V., 1986. Design Sensitivity Analysis of Structural Systems. Academic Press, Orlando.

Hemez, F., 1994. The 3-node composite shell and isoparametric Timoshenko beam elements. In: Report CU-CAS-94-16, Center for Aerospace Structures, University of Colorado, Boulder.

Hyer, M.W., 1981. Calculation of the room-temperature shapes of unsymmetric laminates. Journal of Composite Materials 15, 296–310.

Kemmler, R., 2004. Stabilität und grosse Verchiebungen in der Topologie- und Formoptimierung. In: Report 41, Institute of Structural Mechanics, University of Stuttgart, Germany.

Kleiber, M., Antunez, H., Hien, H., Kowalczyk, P., 1997. Parameter Sensitivity in Nonlinear Mechanics. Wiley, Chichester.

Koester, D.A., Mahadevan, R., Hardy, B., Markus, K.W., 2001. MUMPs™ Design Rules. Cronos Integrated Microsystems, A JDS Uniphase Company, http://www.memsrus.com/cronos/svcsrules.html.

Lee, S.J., Bae, J.E., Hinton, E., 2000. Shell topology optimization using the layered artificial material model. International Journal for Numerical Methods in Engineering 47, 843–867.

Lin, X.Q., Ren, J.G., 1998. Static shape control of laminated plate containing piezoelectric patches. Acta Mechanica Solida Sinica 11, 113–122.

Ma, Z.C., Bradley, E., Peacock, T., Hertzberg, J.R., Lee, Y.C., 2003. Solder-assembled large MEMS flaps for fluid mixing. IEEE Transactions on Advanced Packaging 26, 268–276.

Martin, J.W., Redmond, J.M., Barney, P.S., Henson, T.D., Wehlburg, J.C., Main, J.A., 2000. Distributed sensing and shape control of piezoelectric bimorph mirrors. Journal of Intelligent Material Systems and Structures 11, 744–757.

Martin, J.W., Main, J.A., 2002. Noncontact electron gun actuation of a piezoelectric polymer thin film bimorph structure. Journal of Intelligent Material Systems and Structures 13, 329–337.

Masters, C.B., Salamon, N.J., 1993. Geometrically nonlinear stress–deflection relations for thin film/substrate systems. International Journal of Engineering Science 31, 915–925.

Maute, K., Frangopol, D.M., 2003. Reliability-based design of MEMS mechanisms by topology optimization. Computer and Structures 81, 813–824.

Moulton, T., Ananthasuresh, G.K., 2001. Micromechanical devices with embedded electro-thermal-compliant actuation. Sensors and Actuators A 90, 38–48.

Nix, W.D., 1989. Mechanical properties of thin films. Metallurgical Transactions A 20A, 2217–2245.

Nour-Omid, B., Rankin, C.C., 1991. Finite rotation analysis and consistent linearization using projectors. Computer Methods in Applied Mechanics and Engineering 32, 353–384.

Olhoff, N., Eschenauer, H., 1999. On optimum topology design in mechanics. In: European Conference on Computational Mechanics, August 31–September 3, 1999, München, Germany.

Pedersen, C.B.W., Buhl, T., Sigmund, O., 2001. Topology synthesis of large-displacement compliant mechanisms. International Journal for Numerical Methods in Engineering 50, 2683–2705.

Pedersen, N.L., 2002. Topology optimization of laminated plates with prestress. Computers and Structures 80, 559–570.

Quek, S.T., Wang, S.Y., Ang, K.K., 2003. Vibration control of composite plates via optimal placement of piezoelectric patches. Journal of Intelligent Material Systems and Structures 14, 229–245.

Raulli, M., Maute K., 2004. Topology optimization of electrostatic MEMS. In: AIAA-2004-4335, 10th AIAA/ISSMO Multidisciplinary Analysis and Optimization Conference, August 3–September 1, 2004, Albany, NY.

Rozvany, G.I.N., Zhou, M., Birker, T., 1992. Generalized shape optimization without homogenization. Structural Optimization 10, 250–252.

Salamon, N.J., Masters, C.B., 1995. Bifurcation in isotropic thin film/substrate plate. International Journal of Solids and Structures 32, 473–481.

Schittkowski, K., 1985. NLPQL: a FORTRAN subroutine solving constrained nonlinear programming problems. Annals of Operations Research 5, 485–500.

Sigmund, O., 1994a. Design of material structures using topology optimization. Ph.D. Thesis, Department of Solid Mechanics, Technical University of Denmark.

Sigmund, O., 1994b. Materials with constitutive parameters: an inverse homogenization problem. International Journal of Solids and Structures 31, 2313–2329.

Sigmund, O., 2001a. Design of multiphysics actuators using topology optimization—part 1: one material structures. Computer Methods in Applied Mechanics and Engineering 190, 6577–6604.

Sigmund, O., 2001b. Design of multiphysics actuators using topology optimization—part 2: two material structures. Computer Methods in Applied Mechanics and Engineering 190, 6605–6627.

Sigmund, O., Torquanto, S., 1997. Design of materials with extreme thermal expansion using a three-phase topology optimization method. Journal of the Mechanics and Physics and Solids 45, 1037–1067.

Svanberg, K., 1987. The method of moving asymptotes—a new method for structural optimization. International Journal for Numerical Methods in Engineering 24, 359–373.

Syms, R.R.A., Yeatman, E.M., Bright, V.M., Whitesides, G.M., 2003. Surface tension-powered self-assembly of micro structures—the state-of-the-art. Journal of Microelectromechanical Systems 12, 387–417.

Wang, Q., Wang, C.M., 2000. Optimal placement and size of piezoelectric patches on beams from the controllability perspective. Smart Materials and Structures 9, 558–567.

Wang, X.M., Ehlers, C., Neitzel, M., 1997. An analytical investigation of static models of piezoelectric patches attached to beams and plates. Smart Materials and Structures 6, 204–213.

Xia, Y.N., Whitesides, G.M., 1998. Soft lithography. Annual Review of Materials Science 28, 153–184.

Yin, L., Ananthasuresh, G.K., 2002. A novel topology design scheme for the multi-physics problems of electro-thermally actuated compliant micromechanisms. Sensors and Actuators A 97–98, 599–609.

Zhang, Y., Dunn, M.L., 2003. Deformation of blanketed and patterned bilayer thin film microstructures during post-release thermal and cyclic thermal loading. Journal of Microelectromechanical Systems 12, 788–796.

Zhang, Y., Dunn, M.L., 2004. Geometric and material nonlinearity during the deformation of micron-scale thin-film bilayers subject to thermal loading. Journal of the Mechanics and Physics of Solids 52, 2101–2126.